Available online at www.sciencedirect.com
ScienceDirect
Geochimica et Cosmochimica Acta 70 (2006) 5740–5752
Geochimica
www.elsevier.com/locate/gca

Sulfur isotopic evidence for chemocline upward excursions during the end-Permian mass extinction

Anthony L. Riccardi *, Michael A. Arthur, Lee R. Kump

Department of Geosciences and NASA Astrobiology Institute, The Pennsylvania State University, University Park, PA 16802, USA

Received 16 March 2006; accepted in revised form 4 August 2006

Abstract

The latest Permian was a time of major change in ocean chemistry, accompanying the greatest mass extinction of the Phanerozoic. To examine the nature of these changes, samples from two well-studied marine sections that span the Permian–Triassic boundary have been analyzed: the Meishan and Shangsi sections located in Southern China. Isotopic analysis of the carbonate-associated sulfate in these samples provides a detailed record of several isotopic shifts in $\delta^{34}S_{CAS}$ approaching and across the PTB, ranging from +30 to −15‰ (VCDT), with repeated asynchronous fluctuations at the two locations. We interpret the patterns of isotopic shifts, in conjunction with other data, to indicate a shallow unstable chemocline overlying euxinic deep-water which periodically upwelled into the photic zone. These chemocline upward excursion events introduced sulfide to the photic zone stimulating a bloom of phototrophic sulfur oxidizing bacteria. We hypothesize that elemental sulfur globules produced by these organisms and ^{34}S-depleted pyrite produced in the euxinic water column were deposited in the sediment; later oxidation led to incorporation as CAS. This created the large changes to the $\delta^{34}S_{CAS}$ observed in the latest Permian at these locations.

1. Introduction

The end-Permian interval leading up to the Permian–Triassic boundary (PTB) represents a period of great change in the chemistry of the oceans, as well as the evolution of life on the planet (Benton, 2003). During this interval approximately 50% of marine families and 70% of marine genera went extinct (Erwin, 1993). Additional evidence for terrestrial extinctions across the Permian–Triassic boundary (PTB) implies a change to Earth's entire biosphere (Huey and Ward, 2005). The main pulse of extinction and the initiation of the isotopic shifts occur below the Permian–Triassic boundary (which is defined as the first occurrence of the conodont *Hindeodus parvus*) and the main extinction horizon is often defined as the "event horizon" (Erwin, 1993).

The search for a cause of the end-Permian extinction has long been of intense interest, leading to the generation of numerous hypotheses which invoke both internal and external mechanisms. Hypotheses for internal extinction mechanisms include widespread ocean anoxia (Knoll et al., 1996; Wignall and Twitchett, 1996; Isozaki, 1997), low atmospheric oxygen (Berner, 2005; Huey and Ward, 2005), the development of euxinia in the oceans (Nielsen and Shen, 2004; Grice et al., 2005; Kump et al., 2005), the destabilization of methane clathrates in the oceans (Krull and Retallack, 2000; Krull et al., 2000; Heydari and Hassanzadeh, 2003), and Siberian trap volcanism (Renne and Basu, 1991), among others. External forces have also been invoked as extinction mechanisms, mainly in the form of a bolide impact to the ocean (Becker and Poreda, 2001; Kaiho et al., 2001; Becker et al., 2004), but the evidence for this remains controversial (Koeberl et al., 2004; Renne et al., 2004; Wignall et al., 2004).

Siberian trap volcanism may have been the ultimate trigger for warming-induced anoxia, but low atmospheric oxygen levels may have pre-disposed the ocean to this state

* Corresponding author.
E-mail address: ariccard@geosc.psu.edu (A.L. Riccardi).

0016-7037/$ - see front matter © 2006 Elsevier Inc. All rights reserved.
doi:10.1016/j.gca.2006.08.005

(Berner, 2005). Studies involving numerical models of differing complexity have continued to debate the possibility of ocean-wide anoxia. Some models (Zhang et al., 2001; Winguth and Maier-Reimer, 2005) suggest that the oceans were vigorously circulating during the end-Permian leading to a well-oxygenated Panthalassic ocean. Other studies (Hotinski et al., 2001; Kiehl and Shields, 2005) emphasize that prolonged anoxia or euxinia was primarily the result of warmer deep-water source regions and elevated oceanic phosphate concentrations, rather than a change in the thermohaline overturning rate. The warming of high-latitude surface waters at the end of the Permian would have led to a decrease in the oxygen concentration of deep-water formed in these regions. The more poorly oxygenated waters would then have become rapidly anoxic due to the consumption of oxygen during the oxidation of organic matter sinking from the productive surface waters (Hotinski et al., 2001). Deepening of anoxia led to euxinia and a buildup of dissolved gases (i.e., H_2S, CO_2), in deep-water masses which then resulted in massive upwelling of H_2S and CO_2 (Knoll et al., 1996; Kump et al., 2005).

Sedimentological evidence in support of widespread ocean anoxia has been found at a number of marine sections spanning the late-Permian through early Triassic both in the paleo-Tethys and Panthalassa; see Wignall and Twitchett (2002) for a review. Panthalassic sections from Japan exposed in accreted terranes contain evidence for anoxia from the late-Permian through early Triassic (Isozaki, 1997), while Tethyan sections are characterized by brief intervals of anoxia in shallow-water to deep-water carbonate-rich sections. Some sedimentologic evidence exists for euxinic conditions during the late-Permian for a deep-water Panthalassic section (Nielsen and Shen, 2004) from the late Wujiapingian, and a shallow-water Tethyan section (Wignall et al., 2005) spanning the Permian–Triassic boundary. Pyrite sulfur isotopic data from the deep sea Tanba terrane in Japan (Kajiwara et al., 1994) have been interpreted as representing intensification of euxinia in the Panthalassic Ocean, and shifts in the isotopic composition of carbonate-associated sulfate (CAS) from the Siusi section in Italy (Newton et al., 2004), as well as green sulfur bacteria biomarker evidence from both Meishan in S. China and the Hovea-3 core from W. Australia (Grice et al., 2005) suggest widespread euxinia in the Tethys Ocean during the latest Permian.

The occurrence of large carbon isotope variations during the early Triassic and their relationship to changes in the marine biota as well as sedimentologic evidence (Pruss et al., 2005) shows a prolonged recovery time for the ocean ecosystem after the PTB event, which may mean that the environmental stress which led to the extinction continued well into the Triassic (Payne et al., 2004). The extinction mechanism therefore could have created conditions which prevented the expansion and diversification of many surviving taxa.

The isotopic composition of seawater sulfate, measured from evaporites, reached a Phanerozoic low in the latest Permian (~10‰) and increased to ~30‰ during the earliest Triassic (Strauss, 1997). However, a more recent study reveals that the $\delta^{34}S$ of the oceans may have varied rapidly in the time leading up to the extinction event, suggesting a greater change to the sulfur cycle than had previously been proposed (Newton et al., 2004).

To evaluate this possibility we have analyzed the CAS and pyrite sulfur isotopic compositions from the Meishan and Shangsi sections of south China (Fig. 1). CAS is sulfate which was trapped within the crystal lattice of biogenic and inorganic calcite when it is precipitated and has been shown to record the isotopic composition of seawater sulfate (Burdett et al., 1989; Strauss, 1999). The Meishan and Shangsi sections are both deep-shelf, carbonate-rich sections that span the Permian–Triassic boundary and were located on the Eastern margin of the paleo-Tethys ocean during the latest Permian (Baud et al., 1989; Wignall et al., 1995). We find large uncorrelated fluctuations in CAS $\delta^{34}S$ that require substantial additions of low $\delta^{34}S$

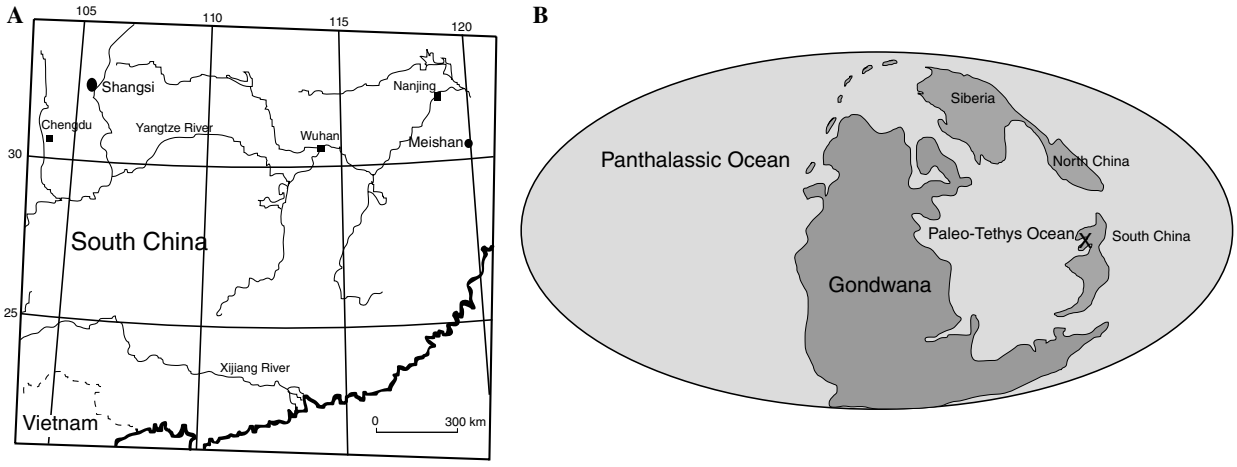

Fig. 1. (A) Modern locations of the Meishan and Shangsi sections, modified after Wignall et al. (1995). (B) Paleogeographic location for the Meishan and Shangsi sections during the late-Permian (255 Ma) is marked X, modified after Scotese (2001).

sulfate either to the basinal waters or diagenetic pore fluids. These patterns indicate that intermittent euxinic conditions were present in the photic zone during the latest Permian and early Triassic in the S. China region, in support of the Kump et al. (2005) hypothesis.

2. Method

2.1. Bulk chemical analyses

An oriented slab from each sample was cut from the main sample and saved for petrographic and geochemical analysis. Acetate peels were prepared after the method of Ali (1968) and petrographically examined for evidence of textural alteration. Bulk chemical analyses were performed on the carbonate fraction of the samples utilizing a Leeman Labs PS3000UV ICP-AES at the Materials Characterization Laboratory at Penn State University with an average analytical uncertainty of ±10 wt% for the calcium and ±5 wt% for trace elements. The material was powdered and dissolved in 5% hydrochloric acid solution. The solution was filtered to remove any insoluble residue and submitted for analysis of Fe, Mn, Sr, and Ca concentrations. CAS and total inorganic carbon concentrations were determined through mass balance during the extraction process. Powdered samples were decarbonated in 25% HCl. Organic carbon and pyrite S concentrations were measured through combustion in a CE Instruments NC2500 elemental analyzer.

2.2. Carbon and oxygen isotopes

Carbonate powders were dissolved individually in an automated common-acid-bath system at 90 °C and analyzed on a Finnigan 252 Mass Spectrometer in the Penn State Stable Isotope Biogeochemistry Laboratory. A laboratory standard was run every seven samples and National Bureau of Standards (NBS) 19 was analyzed at the beginning and end of each run. The variation between replicate analyses was ~0.02‰ and the samples are reported in standard delta notation relative to V-PDB.

We did not perform analyses of the $\delta^{18}O_{CAS}$. However, changes to the $\delta^{18}O_{CAS}$ would be expected to show values similar to those from bacterial sulfide oxidation during a CUE event, and would be indistinguishable from sulfide oxidation occurring later in the sediments making this an unsuitable proxy for determining diagenetic effects in this case.

2.3. Sulfur

CAS was extracted using modified methods from Burdett et al. (1989) and Hurtgen et al. (2002). The limestone samples (50–60 g) were powdered and rinsed with a sodium hypochlorite solution (4–6%) for ~12 h to remove any metastable or organic sulfur compounds. The powder was rinsed multiple times with deionized water (DI) and then dissolved in a 25% HCl solution. The insoluble residue from this dissolution step was rinsed three times with DI and preserved. Saturated barium chloride solution was added to the dissolved fraction to precipitate barite. This solution furnished Ba in excess of that required to precipitate the maximum anticipated sulfate. The solution was heated for ~1 h and set aside for ~12 h. The precipitate (barite) was collected (filtered) the following day. The residue was added to an extraction vessel containing $CrCl_2$ and concentrated HCl and heated to ~120 °C for 1 h. The vessel was purged with nitrogen gas prior to the extraction, and the sulfur was released as H_2S, which flowed through a condenser into a zinc-acetate solution where it precipitated as ZnS (Canfield et al., 1986). A small portion of the barite (~0.30 mg) or zinc sulfide (~0.20 mg) was mixed with five times its weight in V_2O_5 and loaded into 5 × 7 mm tin capsules. The V_2O_5 was added in this ratio because it has been shown to produce consistent $^{18}O/^{16}O$ isotope ratios (Yanagisawa and Sakai, 1983). The $^{34}S/^{32}S$ ratio is affected by the overlapping ion currents produced by $^{32}S^{16}O^{18}O^+$ and $^{34}S^{16}O^{16}O^+$, and through keeping the $^{18}O/^{16}O$ ratio constant, a single correction factor can be applied among all the samples analyzed (Hurtgen et al., 2002). The samples were calibrated against known amounts of NBS-127 barite and internal laboratory standards. The samples were sent to the Stable Isotope Research Facility at Indiana University, Bloomington, IL, for analysis on a VG Optima series II mass spectrometer with the variation between replicate analyses being 0.12‰.

3. Results

The results for the $\delta^{34}S_{CAS}$ of the samples for the Meishan section along with the $\delta^{34}S_{py}$ (pyrite), $\Delta^{34}S$ ($\delta^{34}S_{CAS} - \delta^{34}S_{py}$) and the concentration of CAS and pyrite within the samples can be seen in Fig. 2. The results for these analyses from the Shangsi section are shown in Fig. 3. The concentration and isotopic composition of CAS for both sections varies considerably in the upper Permian and to a lesser extent in the early Triassic. Several values for $\delta^{34}S_{CAS}$ are extremely low (~−20‰) relative to normal seawater values. The changes in $\delta^{34}S_{CAS}$ around the event horizon and PTB at Meishan are similar to those reported in a previous study (Kaiho et al., 2001), but the new data have been collected at higher temporal resolution. CAS $\delta^{34}S$ oscillates between −20 and 20‰ at Meishan with no obvious trend until the event horizon when values plunge to −15‰. The $\delta^{34}S$ of CAS at Shangsi is lower overall for the Permian than at the Meishan section. Changxingian values fluctuate but trend toward less negative values, varying from −10 to 25‰ up-section toward the PTB.

The pyrite sulfur isotopic composition at Meishan is relatively constant before the boundary interval, which is marked by fluctuations. The pyrite sulfur at Shangsi becomes more ^{34}S-enriched approaching the boundary, then drops to values around −40‰ before rapidly returning to −20‰ higher in the section (Fig. 3). The $\Delta^{34}S$ at Shangsi

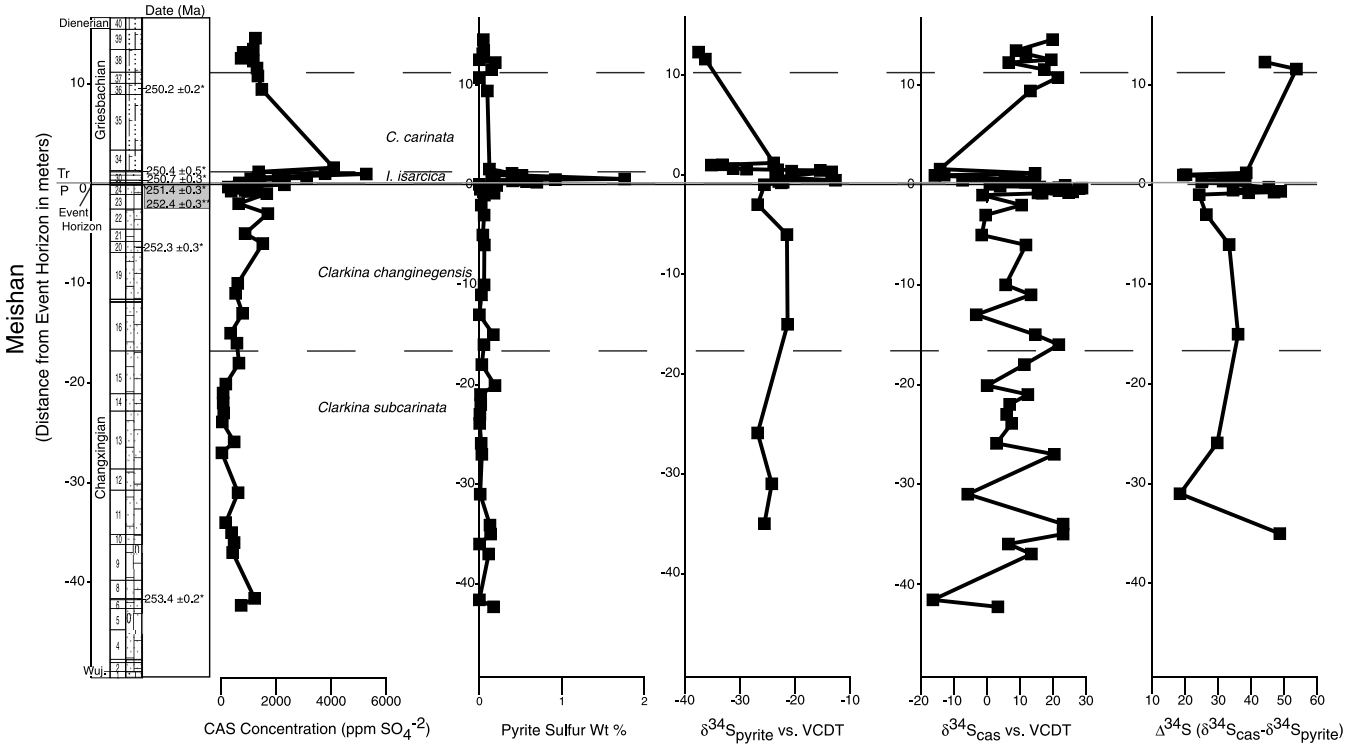

Fig. 2. Isotopic composition of the carbonate-associated sulfate and CAS and pyrite concentration for the Meishan section. Radiometric dates marked with ∗ from Bowring et al. (1998), dates marked with ∗∗ from Mundil et al. (2001). The shaded box shows dates from both sources for the event horizon.

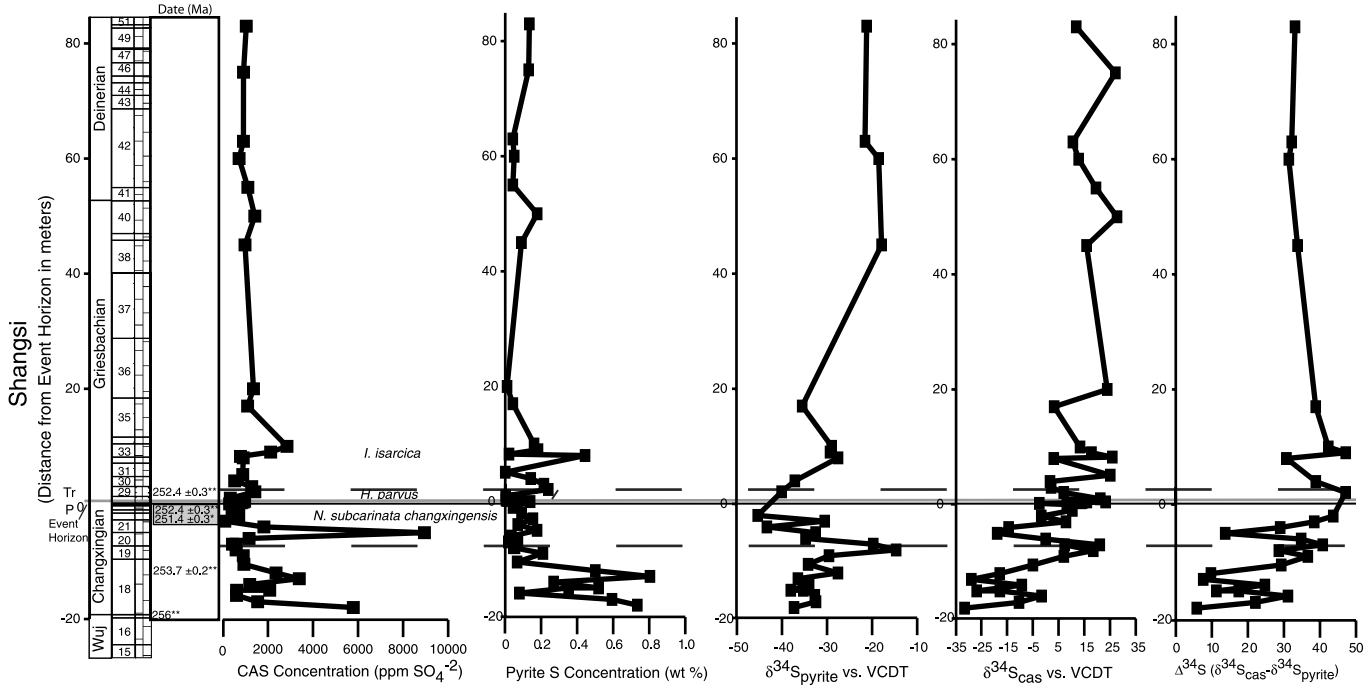

Fig. 3. Isotopic composition of the carbonate-associated sulfate and CAS and pyrite concentration for the Shangsi section. Radiometric dates marked with ∗ from Bowring et al. (1998), dates marked with ∗∗ from Mundil et al. (2001). The shaded box shows dates from both sources for the event horizon.

tracks changes in $\delta^{34}S_{CAS}$ throughout the late-Permian (Fig. 3); the relationship is not as clear in Meishan where fewer pyrite samples were analyzed (Fig. 2). The $\Delta^{34}S$ at Meishan is relatively stable below the boundary at values of about 20–30‰ and increases to 40–50‰ during the extinction event (Fig. 2). The $\Delta^{34}S$ at Shangsi increases

approaching the event from values around 20‰ and also reaches values between 40 and 50‰, at the event horizon, but then remains relatively high into the early Triassic diminishing somewhat toward the top of the measured section. The CAS concentrations at both sections average around 1000–1500 ppm, but a few samples contain significantly higher or lower concentrations of sulfate (Figs. 2 and 3). These samples are of concern because of their anomalous geochemical characteristics: we discuss the possibility of diagenetic alteration below.

The results of the chemical analysis for iron, manganese, and strontium in the acid soluble fraction are shown in Fig. 4. The iron concentration in the samples from both sections increases sharply around the relatively clay-rich beds, but returns to lower values in more carbonate-rich beds above at both sections. Mn/Sr ratios are characterized by a few extremely high values at Meishan in the lower Triassic, but no corresponding change is seen at Shangsi. The Fe/Ca ratios for both sections rise across the event horizon and PTB (Fig. 4). Mn/Ca weight ratios for the majority of the samples at both Meishan and Shangsi (Fig. 4) provide slightly different trends as well. At Shangsi, the Mn/Ca ratio in carbonates increases before the event horizon and then returns to pre-extinction values through the lower Triassic. The samples from higher in the section at Shangsi return to the pre-extinction values. The Mn/Ca values at Meishan remain low up to the event horizon and then increase through the PTB. The Mn/Ca ratios decline higher in the section trending toward pre-extinction values. The Sr/Ca weight ratios for the Meishan section have values ranging from 0.5 to 8 with some values near zero (Fig. 4). For the Shangsi section the Sr/Ca values are as high as 14 with a few smaller values in the lower Triassic (Fig. 4). The data from all of the above figures are presented in electronic annex EA-1.

The lithostratigraphy, micrite texture abundance (based on petrographic analysis of acetate peels), and amount of dolomitization (on the basis of Mg/Ca ratios) are shown in Fig. 5 for both sections. The sections are both composed mainly of limestone, with some dolomite present in bed 27 at Meishan and clay-rich layers near the extinction horizon at both sections. The majority of the samples in the Permian are micritic, and vary between bioturbated and finely laminated with primarily bioturbated intervals present throughout the Permian and close to the PTB. The samples are notably darker in color in the Permian because of somewhat higher total organic carbon contents (TOC) (Fig. 5). Both sections are dominantly micritic in the upper

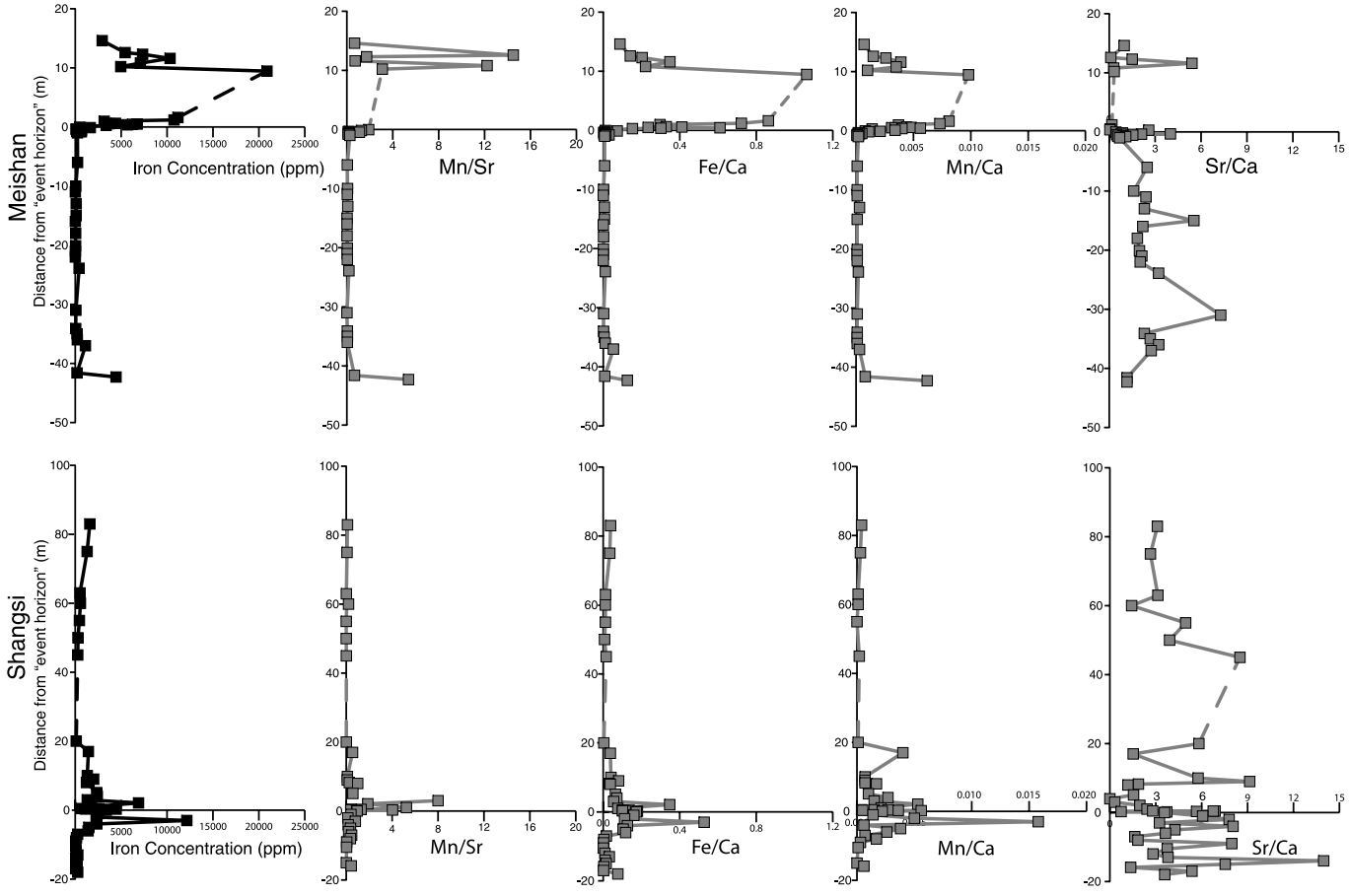

Fig. 4. Stratigraphic profile of the Fe concentration and Mn/Sr, Fe/Ca, Fe/Mn, and Sr/Ca weight ratios for the Meishan and Shangsi sections. Sr/Ca weight ratios have been multiplied by 1000.

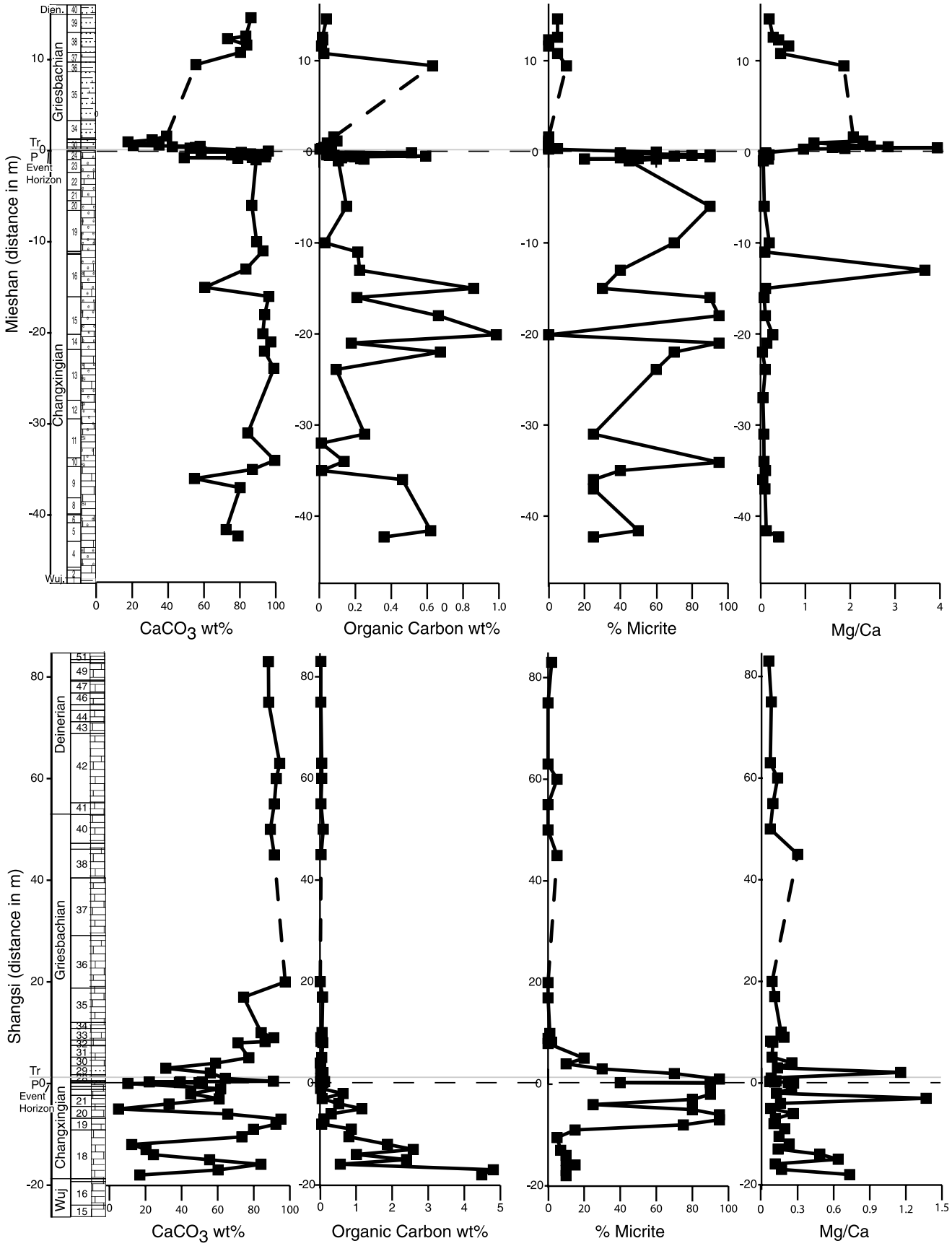

Fig. 5. Stratigraphic profile for the Meishan and Shangsi sections, with the percent calcium carbonate, organic carbon weight percent per sample. The percent of each sample showing a micritic texture was estimated from acetate peel analysis, and the Mg/Ca ratios are shown as a proxy for dolomitization. Note the differing horizontal scales between the two sections for several graphs.

Permian but there is almost no micrite in the lower Triassic with some recrystallization. The lithostratigraphy shown in Fig. 2 for Meishan is from Kexin et al. (1997), and Fig. 3 for Shangsi is from Wignall et al. (1995).

4. Discussion

4.1. Integrity of isotopic compositions

Below we argue that the large asynchronous variations in $\delta^{34}S_{CAS}$ measured at both sections (including large negative values) are the result of very early diagenetic processes driven by fluctuating overlying water-column chemical conditions. In this regard, they are not primary signatures, but they have paleo-environmental significance nonetheless. However, we must rule out other possibilities, including artifacts from sample treatments and significant meteoric and diagenetic influences.

4.1.1. Oxidation during sample digestion

The possibility of pyrite oxidation during sample treatment and digestion remains despite our precautions. However, high pyrite concentrations do not correspond with low values of $\delta^{34}S_{CAS}$ (Fig. 6). Furthermore, the hydrochloric acid used during dissolution has been shown by others (Goldberg et al., 2005) to have no oxidizing effect on pyrite and therefore pyrite oxidation does not contribute to CAS isotopic composition during sample extraction. Neither high apparent Fe concentration (Fig. 7) nor high CAS concentrations (Figs. 8B and 9B) correspond to low $\delta^{34}S_{CAS}$ as might be expected if pyrite oxidation during sample pre-treatment had occurred. Thus, while we cannot rule out pyrite oxidation, we find it unlikely. We are currently performing a comprehensive comparison of various CAS extraction methodologies and will be making a recommendation for standardization of sample processing soon.

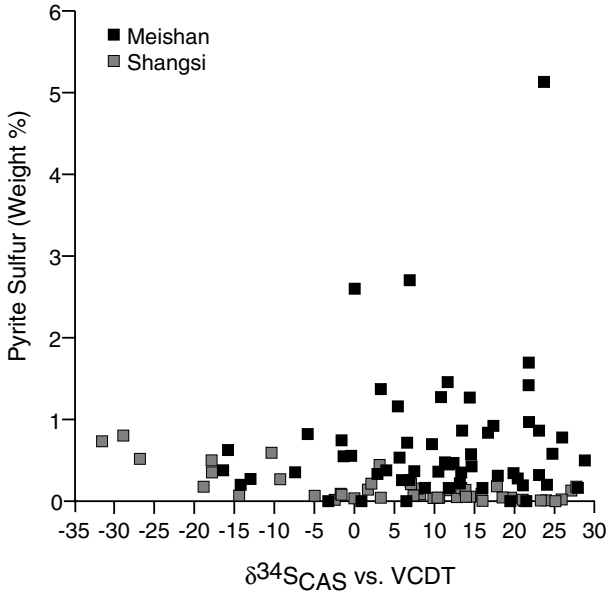

Fig. 6. Pyrite sulfur concentrations from the insoluble residue after decarbonation plotted against the isotopic value of the CAS for both the Meishan and Shangsi sections.

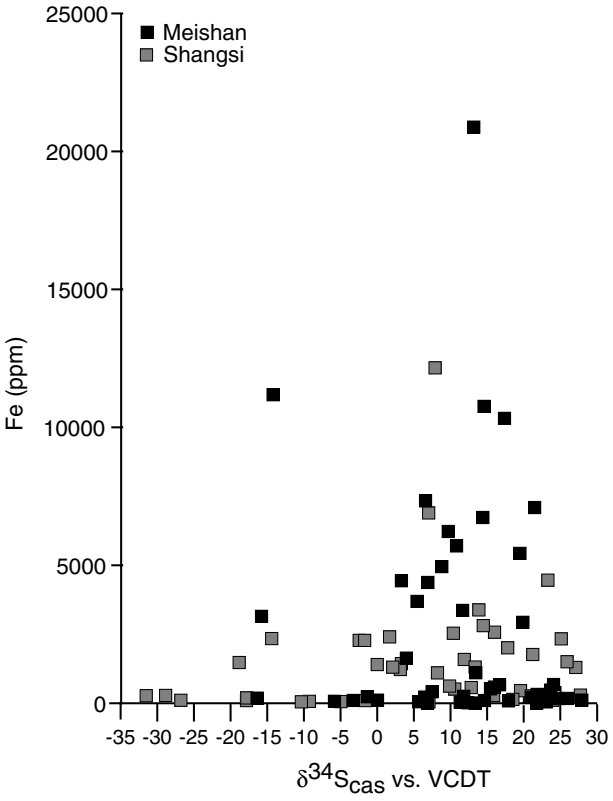

Fig. 7. Iron concentration from the carbonate fraction of the samples for Meishan (dark squares) and Shangsi (grey squares) plotted against the isotopic composition of the CAS.

The Fe/Ca and Mn/Ca ratios for the carbonate fraction of the samples increase approaching (Shangsi) or through (Meishan) the event horizon (Fig. 4). This could reflect a primary trend, the onset of water-column anoxia leading to an increase in the amount of reduced Fe and Mn present during carbonate precipitation. However, the Meishan samples which display the highest Fe/Ca and Mn/Ca ratios also contain higher non-carbonate fractions (Figs. 4 and 5). Thus, the higher Fe and Mn concentrations may be due to Fe and Mn leaching from the clay fraction during hydrochloric acid dissolution. One might expect higher Fe concentrations if pyrite oxidation had taken place, but there is no correspondence between pyrite (sulfur) concentration and HCl-extractable Fe in samples.

4.1.2. Late diagenesis

Oxidation of reduced sulfur compounds and subsequent reincorporation in diagenetic calcite as CAS during early and late diagenesis is another possibility. Although textural evidence mitigates against significant alteration of this type, geochemical evidence can also be brought to bear in the analysis. A crossplot of the $\delta^{13}C_{carb}$ and $\delta^{18}O_{carb}$ exhib-

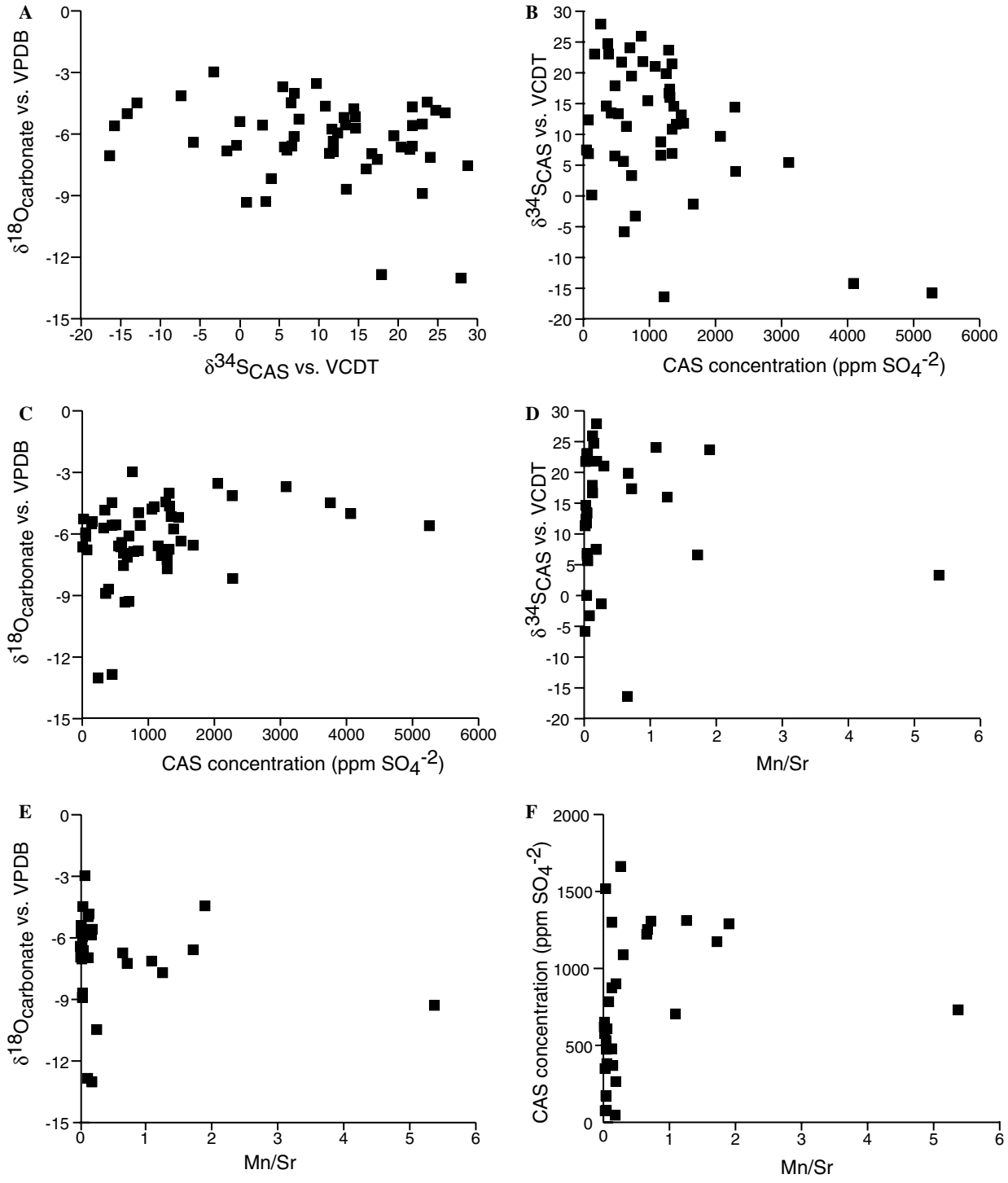

Fig. 8. Elemental and stable isotope analysis for the Meishan section. (A–C) The oxygen isotopes for the carbonates compared to the $\delta^{34}S_{CAS}$ and the CAS concentration. (D) $\delta^{34}S_{CAS}$ vs. the CAS concentration, while E and F compare $\delta^{34}S_{CAS}$ and CAS concentration vs. Mn/Sr.

iting a positive correlation is commonly interpreted as a sign of meteoric diagenesis (Gross and Tracey, 1966; Meyers and Lohmann, 1985), and a plot of $\delta^{18}O_{carb}$ vs. $\delta^{34}S_{CAS}$ yielding a positive correlation would suggest meteoric diagenesis influenced both the carbonate oxygen isotopes and sulfate incorporated in carbonate (Hurtgen et al., 2004) assuming that meteoric waters were much more ^{18}O depleted than the original seawater. No correlation between the $\delta^{18}O_{carb}$ and $\delta^{34}S_{CAS}$ for both the Meishan and Shangsi sections is observed (Figs. 8A and 9A). In addition no relationship is found between $\delta^{18}O_{carb}$ and the CAS concentration for either section (Figs. 8C and 9C).

Some $\delta^{18}O$ values for carbonate at Meishan are extremely low (−10 to −12‰) whereas the $\delta^{18}O$ at Shangsi remains

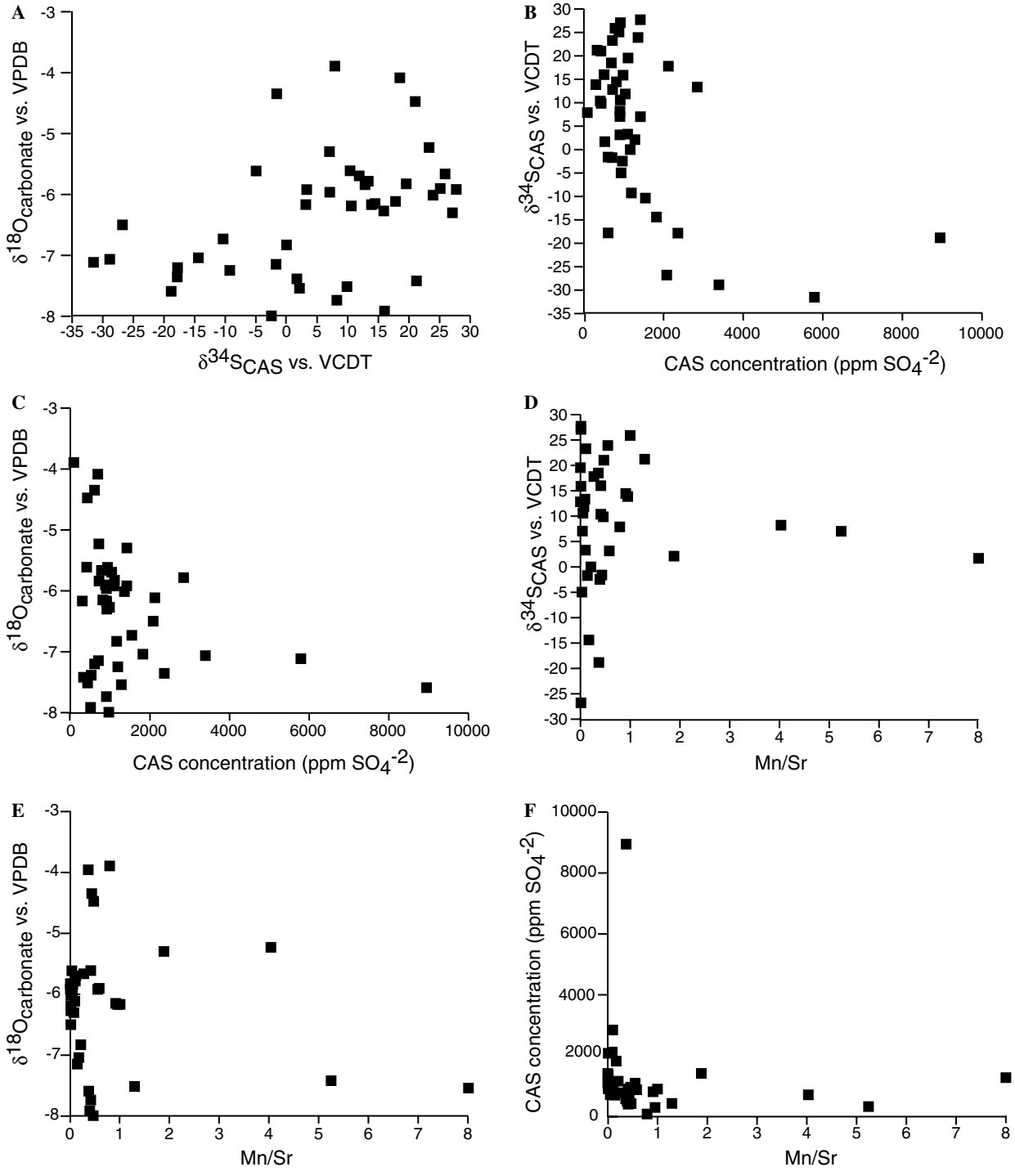

Fig. 9. Elemental and stable isotope analysis for the Shangsi section. (A–C) The oxygen isotopes for the carbonates compared to the $\delta^{34}S_{CAS}$ and the CAS concentration. (D) $\delta^{34}S_{CAS}$ vs. the CAS concentration, while E and F compare $\delta^{34}S_{CAS}$ and CAS concentration vs. Mn/Sr.

between −5 and −8‰. The $\delta^{18}O$ trend in apparently reasonably preserved Phanerozoic marine carbonates, while increasing since the Precambrian, exhibits lower values around the PTB with a lowest value of ~ −10‰ and a mean value of −7‰ (Veizer et al., 1999). The overall trend suggests that most of the $\delta^{18}O$ values reported here are within the average for this time period. The only samples which lie far outside this range are two values at Meishan which do not occur in samples with low $\delta^{34}S_{CAS}$ values. Crossplots of the isotopic composition of carbonate-carbon and carbonate-oxygen are shown in Fig. 10. As with the other plots, no discernable trend is visible.

As an additional test of alteration the $\delta^{18}O_{carb}$, $\delta^{34}S_{CAS}$, and CAS concentration were plotted against Mn/Sr ratios for all samples (Hurtgen et al., 2004). Strontium is often removed during diagenesis while Mn is enriched resulting in

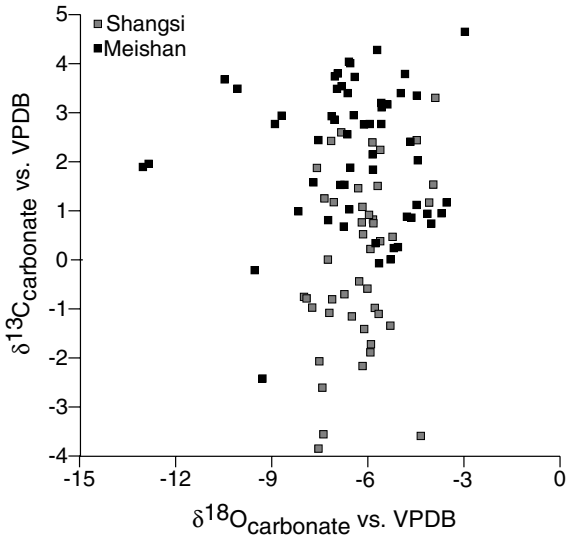

Fig. 10. Crossplots of the carbonate-carbon and carbonate-oxygen isotopic values for both Meishan and Shangsi are shown above. Meishan carbonate-carbon isotopic values are from Jin et al. (2000) and were performed on the same sample set; all other values are from this study.

higher Mn/Sr ratios and low Sr/Ca ratios (Hurtgen et al., 2004). The crossplots against the Mn/Sr ratios for both Meishan (Figs. 8D–F) and Shangsi (Figs. 9D–F) provide no correlation to suggest diagenetic influence. From the partition coefficient and today's seawater Sr/Ca ratio (Bathurst, 1971) calcite is expected to have Sr/Ca equal to 1.2 mmol/mol. The majority of the samples are above this value, with some exceptions near the PTB (Fig. 4), suggesting that the Meishan and Shangsi samples as a whole were only moderately diagenetically altered. That is, the samples experienced compaction and cementation but not wholesale dissolution, reprecipitation, or major pore filling cementation. Those samples with low Sr/Ca values also do not have extremely low values for $\delta^{34}S_{CAS}$.

4.1.3. Early marine diagenesis

The low values of $\delta^{34}S_{CAS}$ in some samples and the significant fluctuations of $\delta^{34}S$ at both sampled locations are most likely not the result of meteoric diagenesis (exposure, freshwater circulation, and/or deep meteoric events). They are also not likely to represent variations in the global oceanic value, most simply because they do not correlate between the two sections. However, diagenesis that reflects changes in primary environmental conditions may play an important role. Local addition of ^{34}S-depleted sulfur to the sediment, either immediately upon deposition or somewhat later as an early seafloor diagenetic overprint may have played an important role. Petrographic examination of acetate peels exhibited evidence for recrystallization although the samples were dominantly micritic. However, CAS in lime-mud has been shown to be remarkably resistant to alteration during early diagenesis, even in the presence of large quantities of organic matter and sulfate-reducing bacteria in pore water (Lyons et al., 2004). It is important to note that the Lyons et al. (2004) study was conducted in Florida Bay, which is well oxygenated. In contrast, the Meishan and Shangsi seafloors are interpreted to have been episodically overlain by euxinic watermasses. If so, reduced sulfur minerals precipitated in the water column, with low values of $\delta^{34}S$, could have been episodically deposited in the sediments. If the overlying waters became oxygenated during the intervals between euxinia, oxygen could have diffused into the sediment, oxidizing the reduced sulfur minerals and releasing ^{34}S-depleted sulfate into the pore water. The product sulfate could have later become incorporated into the limestone as CAS, if the carbonate sediments were able to buffer the acidity created by the oxidation of pyrite.

The pyrite sulfur concentration in samples throughout each section remains fairly consistent and does not correlate with changes to $\delta^{34}S_{CAS}$ (Fig. 6). The samples with the most depleted $\delta^{34}S$ values also contain some of the lowest iron concentrations suggesting that an alternative source for the addition of ^{34}S-depleted sulfur must be considered to fully explain the changes to $\delta^{34}S_{CAS}$.

4.1.4. Summary of diagenesis

From the above petrographic, chemical, and isotopic analyses, we conclude that early diagenetic alteration may have played a primary role in creating the rapid shifts observed in $\delta^{34}S_{CAS}$ at both sections. However, this proposed early diagenetic alteration is considered to be a direct result of rapid environmental variations (oxic–anoxic cycles). The extremely light values for the CAS sulfur isotopes and the recrystallization textures petrographically observed in many samples are consistent with early marine diagenesis. Geochemical evidence suggests that later diagenesis and meteoric diagenesis are unlikely to explain the observed changes and pyrite alone as the source of this ^{34}S-depleted sulfate is not the sole source of additional sulfur because rapid changes in $\delta^{34}S_{CAS}$ occur despite relatively constant pyrite sulfur concentrations. While not necessarily representing the original surface-water $\delta^{34}S$ values, the $\delta^{34}S_{CAS}$ indicate a change to the sulfur input to the sediments during the end-Permian and early Triassic that may provide a clue to the environmental changes occurring at this time.

4.2. Euxinia

Numerical modeling has shown that the deep-water of the ocean could have become euxinic during periods of prolonged anoxia such as the end Permian (Hotinski et al., 2001), and that the chemocline between the oxygenated surface waters and the sulfide-rich deep-water could become unstable with H_2S concentrations higher than 1 mmol/kg (Kump et al., 2005). This would have led to chemocline upward excursion (CUE) events where sulfidic deep-water would be transferred to the shelf environment and hydrogen sulfide would be released to the atmosphere (Kump et al., 2005).

4.2.1. CUE events and sulfur isotopes

Sulfide in the euxinic deep-water would have been ^{34}S-depleted, being derived from bacterial sulfate reducers thriving in anoxic waters. Newton et al. (2004) suggested that a reduction of 30% of oceanic sulfate to sulfide and storage of this sulfide in euxinic deep-waters would be enough to produce the shifts between 11.5 and 27‰ they observe in $\delta^{34}S_{CAS}$. The problem with this mechanism is that isotopically light sulfide upwelling into the photic zone would be accompanied by isotopically heavy sulfate resulting from Rayleigh distillation isotope effects during water-column sulfate reduction. Upon oxidation the two would mix creating a parcel of water that had the original (undistilled) seawater value. Thus, we must find other mechanisms for preservation of the light sulfur isotope values. In other words, we must identify mechanisms for sequestering the isotopically light sulfur before it oxidizes and mixes with the accompanying isotopically heavy deep-water sulfate.

4.2.2. The effect of CUE events on sediment chemistry

One method for sequestering the sulfide is for bacteria or inorganic geochemical reactions to immediately convert it into a relatively insoluble phase (elemental sulfur or pyrite) under euxinic conditions. The episodic excursions of euxinic water in the photic zone proposed by Kump et al. (2005) would have led to conditions favorable for blooms of phototrophic purple and green sulfur bacteria. Elemental sulfur derived from this bacterial source would have been isotopically depleted in ^{34}S, being derived from an isotopically light source and potentially subjected to subsequent disproportionation during oxidation. Disproportionation reactions (cycling sulfur between sulfide and elemental sulfur) could have occurred in a shallow chemocline creating ^{34}S-depleted sulfides and the large $\Delta^{34}S$ values (Figs. 2 and 3; Canfield and Thamdrup, 1994). The elemental sulfur produced in the water column would have fallen to the ocean floor and become incorporated into the surface sediments. Sulfur globules have been shown to form in the surface waters off the coast of Namibia during build up and release of H_2S from the sediments (Weeks et al., 2004). These elemental sulfur globules have been mapped in satellite images being transported along the coast for later deposition (Weeks et al., 2004), similar to the mechanism being suggested here for the end-Permian. In the presence of ferrous iron, some of the upwelling sulfur might have also been sequestered as FeS or FeS_2 and deposited in the sediments, to later become oxidized. However, due to the lack of a correlation between Fe and $\delta^{34}S_{CAS}$ and other limitations on pyrite as the source of sulfur discussed above, we favor elemental S as the primary shuttle of low $\delta^{34}S$ sulfur to the sediments.

The values for $\delta^{34}S_{CAS}$ at Meishan and Shangsi reach a maximum just before the event horizon, coinciding with both the biomarker evidence for green sulfur bacteria (Grice et al., 2005) and with the highest values for $\Delta^{34}S$ at both sections, and then fall to extremely low values across the extinction horizon (Figs. 2 and 3). Evaporite sulfur $\delta^{34}S_{CAS}$ values representing open oceanic sulfate reach a minimum in the late-Permian (~12‰) and trend towards heavier values through the latest Permian and into the Triassic where they reach a high of ~25‰ (Kampschulte and Strauss, 2004). The values measured at both Meishan and Shangsi (Figs. 2 and 3) trend toward the extrapolated evaporite curve while repeatedly deviating to more ^{34}S-depleted values throughout the latest Permian, which we hypothesize to indicate repeated CUE events in this region.

At the end of the CUE events, the sediment-water-interface (SWI) would have become oxic, leading to the oxidation of the elemental sulfur and some of the pyrite (or Fe monosulfide precursors) creating pore waters with low pH. These low pH waters would have driven recrystallization, by dissolving portions of the lime-mud sediments until the carbonate system was able to buffer the acidity and allow for precipitation of secondary (diagenetic) carbonate incorporating ^{34}S-depleted sulfate as CAS. Assuming that 1 wt% of the sediments was elemental sulfur formed within the water column, approximately 20,000 ppm of ^{34}S-depleted sulfate could have been generated. With the average CAS concentration within the primary micrite being ~1000 ppm (Figs. 2 and 3) the sulfate within the sediments would have been overwhelmed, thereby creating the isotopically light signals observed. While this is technically a "diagenetic" effect, it is driven by the input of sulfur from the CUE events providing evidence of photic zone euxinia.

A small decrease in the $\delta^{34}S_{CAS}$ also occurs at the PTB, which is the second location at Meishan where green sulfur bacteria biomarkers were detected indicating a second major bloom of phototrophic sulfur bacteria as the result of euxinia in the photic zone (Grice et al., 2005). These results are consistent with those of Pruss et al. (2005) and Payne et al. (2004) which indicate that anoxia and, now, perhaps euxinia continued well into the early Triassic and impeded the biotic recovery from the end-Permian mass extinction.

5. Conclusions

The large amplitude, apparently rapid variations in $\delta^{34}S_{CAS}$ measured in this study indicated that multiple chemocline upward excursion (CUE) events occurred in S. China and likely elsewhere during the end-Permian mass extinction. Repeated changes in the oxidation state of the uppermost sediments due to the incursion and retreat of euxinic waters onto the continental shelf led to the generation of considerable quantities of reduced sulfur minerals (elemental and pyrite S). These reduced sulfur minerals were deposited in surface sediments during CUE events and then oxidized as euxinic waters retreated to the deep sea. As a result the sulfur isotopic composition of the sulfate trapped in carbonate minerals underwent large, local fluctuations. The inferred changes to the sulfur cycle during the end-Permian strongly suggest that an internal mechanism was the trigger for the extinction and that the perturbations began before the main pulse of extinction and continued well into the Triassic.

Acknowledgments

We thank Steven D'Hondt at the University of Rhode Island for providing the Meishan and Shangsi samples, Jon Fong at the stable isotope research facility at Indiana University, Bloomington for sulfur isotope analyses, Dennis Walizer (Penn State University, Stable Isotope Lab) for his assistance on the mass spectrometer during carbonate analyses, Hiroshi Ohmoto for laboratory access through the Penn State Astrobiology Research Center, Theresa Menotti for her assistance in sample preparation, and Martin Schoonen for laboratory access and assistance. This manuscript was improved by comments from Matt Hurtgen and an anonymous reviewer. This work was funded by NSF EAR-0208119 and represents a collaboration facilitated by the NASA Astrobiology Institute through NASA cooperative agreement, Grant No. NNA04CC06A. This research was also supported by the NSF (IGERT) grant DGE-9972759.

Associate editor: Donald E. Canfield

Appendix A. Supplementary data

Supplementary data associated with this article can be found, in the online version, at doi:10.1016/j.gca.2006.08.005.

References

Ali, S.A., 1968. Acetate peels for the study of carbonate rocks. *Pak. J. Sci. Ind. Res.* **11** (2), 213–214.

Bathurst, R.G.C., 1971. Some chemical considerations*Carbonate Sediments and Their Diagenesis*, vol. 12. Elsevier Publishing Company, pp. 231–294.

Baud, A., Magaritz, M., Holser, W.T., Rehovot, E., 1989. Permian–Triassic of the Tethys: carbon isotope studies. *Geol. Rundsch.* **78** (2), 649–677.

Becker, L., Poreda, R.J., 2001. Fullerene and mass extinction in the geologic record. Meteorit. Planet. Sci. 36 (9), Suppl., pp.17, A17.

Becker, L., Poreda, R.J., Basu, A.R., Pope, K.O., Harrison, T.M., Nicholson, C., Iasky, R., 2004. Bedout: a possible end-Permian impact crater offshore of Northwestern Australia. *Science* **304** (5676), 1469–1477.

Benton, M.J., 2003. *When Life Nearly Died*. Thames & Hudson Ltd.

Berner, R.A., 2005. The carbon and sulfur cycles and atmospheric oxygen from middle Permian to middle Triassic. *Geochim. Cosmochim. Acta* **69** (13), 3211–3217.

Bowring, S.A., Erwin, D.H., Jin, Y.G., Martin, M.W., Davidek, K., Wang, W., 1998. U/Pb Zircon Geochronology and tempo of the end-Permian mass extinction. *Science* **280**, 1039–1045.

Burdett, J.W., Arthur, M.A., Richardson, M., 1989. A Neogene seawater sulfur isotope age curve from calcareous pelagic microfossils. *Earth Planet. Sci. Lett.* **94**, 189–198.

Canfield, D.E., Raiswell, R., Westrich, J.T., Reaves, C.M., Berner, R.A., 1986. The use of chromium reduction in the analysis of reduced inorganic sulfur in sediments and shales. *Chem. Geol.* **54** (1–2), 149–155.

Canfield, D.E., Thamdrup, B., 1994. The production of ^{34}S-depleted sulfide during bacterial disproportionation of elemental sulfur. *Science* **266**, 1973–1975.

Erwin, D.H., 1993. *The Great Paleozoic Crisis: Life and Death in the Permian*. Columbia University Press.

Goldberg, T., Poulton, S.W., Strauss, H., 2005. Sulphur and oxygen isotope signatures of late Neoproterozoic to early Cambrian sulphate, Yangtze Platform, China: diagenetic constraints and seawater evolution. *Precambrian Res.* **137** (3–4), 223–241.

Grice, K., Cao, C.Q., Love, G.D., Bottcher, M., Twitchett, R.J., Grosjean, E., Summons, R., Turgeon, S., Dunning, W., Jin, Y., 2005. Photic zone euxinia during the Permian–Triassic superanoxic event. *Science* **307**, 706–709.

Gross, M.G., Tracey, J.I., 1966. Oxygen and carbon isotopic composition of limestones and dolomites, bikini and eniwetok atolls. *Science* **151** (3714), 1082–1084.

Heydari, E., Hassanzadeh, J., 2003. Deev Jahi model of the Permian–Triassic boundary mass extinction: a case for gas hydrates as the main cause of biological crisis on Earth. *Sediment. Geol.* **163**, 147–163.

Hotinski, R.M., Bice, K.L., Kump, L.R., Naijar, R.G., Arthur, M.A., 2001. Ocean stagnation and end-Permian anoxia. *Geology* **29** (1), 7–10.

Huey, R.B., Ward, P.D., 2005. Hypoxia, global warming, and terrestrial Late Permian extinctions. *Science* **308**, 398–401.

Hurtgen, M.T., Arthur, M.A., Prave, A.R., 2004. The sulfur isotope composition of carbonate-associated sulfate in Mesoproterozoic to Neoproterozoic carbonates from Death Valley, California. In: J.P. Amend, K.J. Edwards, T.W. Lyons. (Eds.), Sulfur Biogeochemistry—Past and Present, vol. 379. Geological Society of America Special Paper.

Hurtgen, M.T., Arthur, M.A., Suits, N.S., Kaufman, A.J., 2002. The sulfur isotopic composition of Neoproterozoic seawater sulfate: implications for a snowball Earth? *Earth Planet. Sci. Lett.* **203**, 413–430.

Isozaki, Y., 1997. Permo-Triassic boundary superanoxia and stratified superocean: records from lost deep-sea. *Science* **276**, 235–238.

Jin, Y.G., Wang, Y., Shang, Q.H., Cao, C.Q., Erwin, D.H., 2000. Pattern of marine mass extinction near the Permian–Triassic boundary in South China. *Science* **289**, 432–436.

Kaiho, K., Kajiwara, Y., Nakano, T., Miura, Y., Kawahata, H., Tazaki, K., Ueshima, M., Chen, Z., Shi, G.R., 2001. End-Permian catastrophe by a bolide impact: evidence of a gigantic release of sulfur from the Mantle. *Geology* **29** (9), 815–818.

Kajiwara, Y., Yamakita, S., Ishida, K., Ishiga, H., Imai, A., 1994. Development of a largely anoxic stratified ocean and its temporary massive mixing at the Permian/Triassic boundary supported by the sulfur isotope record. *Palaeogeogr. Palaeoclimatol. Palaeoecol.* **111**, 367–379.

Kampschulte, A., Strauss, H., 2004. The Sulfur isotopic evolution of Phanerozoic seawater based on the analysis of structurally substituted sulfate in carbonates. *Chem. Geol.* **204**, 255–286.

Kexin, Z., Jinnan, T., Hongfu, Y., Shunbao, W., 1997. Sequence stratigraphy of the Permian–Triassic boundary section of Changxing, Zhejiang, Southern China. *Acta Geol. Sin. (English Version)* **71** (4), 90–103.

Kiehl, J.T., Shields, C.A., 2005. Climate simulation of the latest Permian: implications for mass extinction. *Geology* **33** (9), 757–760.

Knoll, A.H., Bambach, R.K., Canfield, D.E., Grotzinger, J.P., 1996. Comparative earth history and Late Permian mass extinction. *Science* **273**, 452–457.

Koeberl, C., Farley, K.A., Peucker-Ehrenbrink, B., Sephton, M.A., 2004. Geochemistry of the end-Permian extinction event in Austria and Italy: no evidence for an extraterrestrial component. *Geology* **32** (12), 1053–1056.

Krull, E.S., Retallack, G.J., 2000. δ^{13}C depth profiles from paleosols across the Permian–Triassic boundary: evidence for methane release. *GSA Bull.* **112** (9), 1459–1472.

Krull, E.S., Retallack, G.J., Campbell, I.H., Lyon, G.L., 2000. $\delta^{13}C_{org}$ chemostratigraphy of the Permian–Triassic boundary in the Maitai Group, New Zealand: evidence for high-latitudinal methane release. *NZ J. Sci.* **43**, 23–32.

Kump, L.R., Pavlov, A., Arthur, M.A., 2005. Massive release of hydrogen sulfide to the surface ocean and atmosphere during intervals of oceanic anoxia. *Geology* **33** (5), 397–400.

Lyons, T.W., Walter, L.M., Gellatly, A.M., Martini, A.M., Blake, R.E., 2004. Sites of anomalous organic remineralization in the carbonate sediments of South Florida, USA: The sulfur cycle and carbonate-associated sulfate. In: J.P. Amend, K.J. Edwards, T.W. Lyons (Eds.), Sulfur Biogeochemistry—Past and Present, vol. 379, pp. 161–176. Geological Society of America Special Papers.

Meyers, W.J., Lohmann, K.C., 1985. Isotope geochemistry of regionally extensive calcite cement zones and marine components in Mississippian limestones, New Mexico. In: Schneidermann, N. Harris, P.M. (Eds.), Carbonate Cements, vol. 36, pp. 223–239. SEPM Special Publications.

Mundil, R., Metcalfe, I., Ludwig, K.R., Renne, P.R., Oberli, F., Nicoll, R.S., 2001. Timing of the Permian–Triassic biotic crisis: implications from new zircon U/Pb age data (and their limitations). *Earth Planet. Sci. Lett.* **187**, 131–145.

Newton, R.J., Pevitt, E.L., Wignall, P., Bottrell, S.H., 2004. Large shifts in the isotopic composition of seawater sulphate across the Permo-Triassic boundary in northern Italy. *Earth Planet. Sci. Lett.* **218**, 1–15.

Nielsen, J.K., Shen, Y., 2004. Evidence for sulfidic deep water during the Late Permian in the East Greenland Basin. *Geology* **32** (12), 1037–1040.

Payne, J.L., Lehrmann, D.J., Wei, J., Orchard, M.J., Schrag, D.P., Knoll, A.H., 2004. Large perturbations of the carbon cycle during recovery from the End-Permian extinction. *Science* **305**, 506–509.

Pruss, S.B., Corsetti, F.A., Bottjer, D.J., 2005. The unusual sedimentary rock record of the Early Triassic: a case study from the southwestern United States. *Palaeogeogr. Palaeoclimatol. Palaeoecol.* **222** (1–2), 33–52.

Renne, P.R., Basu, A.R., 1991. Rapid eruption of the Siberian traps flood basalts at the Permo-Triassic boundary. *Science* **253**, 176–179.

Renne, P.R., Melosh, H.J., Farley, K.A., Reimold, W.U., Koeberl, C., Rampino, M.R., Kelly, S.P., Ivanov, B., 2004. Is bedout an impact crater? Take 2. *Science* **306** (5696), 611–612.

Scotese, C.R., 2001. *Atlas of Earth History, volume 1—Paleogeography*. Paleomap Project, Arlington, TX, 52pp.

Strauss, H., 1997. The isotopic composition of sedimentary sulfur through time. *Palaeogeogr. Palaeoclimatol. Palaeoecol.* **132**, 97–118.

Strauss, H., 1999. Geological evolution from isotope proxy signals—sulfur. *Chem. Geol.* **161**, 89–101.

Veizer, J., Ala, D., Azmy, K., Bruckschen, P., Buhl, D., Bruhn, F., Carden, G.A.F., Diener, A., Ebneth, S., Godderis, Y., Jasper, T., Korte, C., Pawellek, F., Podlaha, O.G., Strauss, H., 1999. $^{87}Sr/^{86}Sr$, $\delta^{13}C$, and $\delta^{18}O$ evolution of Phanerozoic seawater. *Chem. Geol.* **161**, 59–88.

Weeks, S.J., Currie, B., Bakun, A., Peard, K.R., 2004. Hydrogen sulphide eruptions in the Atlantic Ocean off southern Africa: implications of a new view based on SeaWiFS satellite imagery. *Deep Sea Res. Part I: Oceanogr. Res. Pap.* **51** (2), 153–172.

Wignall, P., Hallam, A., Xulong, L., Fengqing, Y., 1995. Palaeoenvironmental changes across the Permian/Triassic boundary at Shangsi (N. Sichuan, China). *Hist. Biol.* **10**, 175–189.

Wignall, P., Newton, R.J., Brookfield, M.E., 2005. Pyrite framboid evidence for oxygen-poor deposition during the Permian–Triassic crisis in Kashmir. *Palaeogeogr. Palaeoclimatol. Palaeoecol.* **216**, 183–188.

Wignall, P., Thomas, B., Willink, R.J., Watling, J., 2004. Is bedout an impact crater? Take 1. *Science* **306** (5696), 609–610.

Wignall, P., Twitchett, R.J., 1996. Oceanic anoxia and the end Permian mass extinction. *Science* **272**, 1155–1158.

Wignall, P., Twitchett, R.J., 2002. Extent, duration, and nature of the Permian-Triassic superanoxic event. *Geol. Soc. Am. Spec. Pap.* **356**, 395–413.

Winguth, A.M.E., Maier-Reimer, E., 2005. Causes of the marine productivity and oxygen changes associated with the Permian–Triassic boundary: a reevaluation with ocean general circulation models. *Mar. Geol.* **217** (3–4), 283–304.

Yanagisawa, F., Sakai, H., 1983. Thermal decomposition of barium sulfate–vanadium pentoxide–silica glass mixtures for preparation of sulfur dioxide in sulfur isotope ratio measurements. *J. Anal. Chem.* **55**, 985–987.

Zhang, R., Follows, M.J., Grotzinger, J.P., Marshall, J., 2001. Could the Late Permian deep ocean have been anoxic? *Paleoceanography* **16** (3), 317–329.